J Biomol NMR (2015) 61:7–20
DOI 10.1007/s10858-014-9875-6

ARTICLE

Combined zero-quantum and spin-diffusion mixing for efficient homonuclear correlation spectroscopy under fast MAS: broadband recoupling and detection of long-range correlations

Xingyu Lu · Changmiao Guo · Guangjin Hou · Tatyana Polenova

Received: 31 July 2014 / Accepted: 14 October 2014 / Published online: 25 November 2014

Abstract Fast magic angle spinning (MAS) NMR spectroscopy is emerging as an essential analytical and structural biology technique. Large resolution and sensitivity enhancements observed under fast MAS conditions enable structural and dynamics analysis of challenging systems, such as large macromolecular assemblies and isotopically dilute samples, using only a fraction of material required for conventional experiments. Homonuclear dipolar-based correlation spectroscopy constitutes a centerpiece in the MAS NMR methodological toolbox, and is used essentially in every biological and organic system for deriving resonance assignments and distance restraints information necessary for structural analysis. Under fast MAS conditions (rotation frequencies above 35–40 kHz), dipolar-based techniques that yield multi-bond correlations and non-trivial distance information are ineffective and suffer from low polarization transfer efficiency. To overcome this limitation, we have developed a family of experiments, CORD–RFDR. These experiments exploit the advantages of both zero-quantum RFDR and spin-diffusion based CORD methods, and exhibit highly efficient and broadband dipolar recoupling across the entire spectrum, for both short-range and long-range correlations. We have verified the performance of the CORD–RFDR sequences experimentally on a U-^{13}C,^{15}N-MLF tripeptide and by numerical simulations. We demonstrate applications of 2D CORD–RFDR correlation spectroscopy in dynein light chain LC8 and HIV-1 CA tubular assemblies. In the CORD–RFDR spectra of LC8 acquired at the MAS frequency of 40 kHz, many new intra- and inter-residue correlations are detected, which were not observed with conventional dipolar recoupling sequences. At a moderate MAS frequency of 14 kHz, the CORD–RFDR experiment exhibits excellent performance as well, as demonstrated in the HIV-1 CA tubular assemblies. Taken together, the results indicate that CORD–RFDR experiment is beneficial in a broad range of conditions, including both high and moderate MAS frequencies and magnetic fields.

Keywords $R2_n^v$-Driven Spin Diffusion (RDSD) · COmbined $R2_n^v$-Driven Spin Diffusion (CORD SD) · Radio frequency driven recoupling (RFDR) · Symmetry sequences · Solid-state NMR · Fast MAS · Broadband homonuclear correlation spectroscopy

Xingyu Lu and Changmiao Guo have contributed equally to this work.

Electronic supplementary material The online version of this article (doi:10.1007/s10858-014-9875-6) contains supplementary material, which is available to authorized users.

X. Lu · C. Guo · G. Hou · T. Polenova
Department of Chemistry and Biochemistry, University of Delaware, Newark, DE 19716, USA
e-mail: luxingyu@udel.edu

C. Guo
e-mail: cmguo@udel.edu

X. Lu · G. Hou (✉) · T. Polenova (✉)
Pittsburgh Center for HIV Protein Interactions, University of Pittsburgh School of Medicine, Pittsburgh, PA 15261, USA
e-mail: hou@udel.edu

T. Polenova
e-mail: tpolenov@udel.edu

Introduction

Magic angle spinning (MAS) NMR spectroscopy is a method of choice for structural and dynamics characterization of large macromolecular assemblies that are

intractable by traditional structural biology techniques, such as inherently insoluble proteins and protein assemblies lacking long-range order (Han et al. 2013; McDermott 2009; Renault et al. 2010; Sun et al. 2012a; Tycko 2011; Yang et al. 2008). In biomolecular MAS NMR, resonance assignments and distance restraints are usually gained from multidimensional dipolar-based experiments, which yield either hetero- or homonuclear through-space correlations. Of these methods, homonuclear correlation spectroscopy is an essential tool for deriving information on interatomic proximities, which plays a key role in the protein structure determination as well as studies of internal dynamics. Fast MAS frequencies (40–110 kHz) are increasingly used for recording homonuclear correlation spectra with high resolution and, in conjunction with magnetic fields of 17.6 T and above, are advantageous for analysis of large biological systems. Under the conditions of high magnetic fields and fast MAS frequencies, two challenges arise in homonuclear dipolar-based experiments: (1) the ^{13}C isotropic chemical shift range covers the frequency range of 40–50 kHz making it difficult to attain uniform polarization transfer across the entire spectrum; and (2) conventional second-order dipolar recoupling sequences used for recording long-range distance restraints fail at fast MAS frequencies. The homonuclear correlation experiments developed recently with the goal to overcome the above obstacles have relatively low transfer efficiencies that scale with the inverse of the MAS frequency (Hou et al. 2011, 2013; Hu et al. 2011, 2012; Ladizhansky 2009; Weingarth et al. 2009).

Different dipolar recoupling sequences have been established for recording through-space homonuclear correlations, including zero-quantum and proton-assisted spin diffusion schemes. The zero-quantum (1st-order recoupling) methods, such as DREAM (Ernst et al. 2004), RFDR (Bennett et al. 1992) and fpRFDR (Fig. 1a) (Brinkmann et al. 2002; Ishii 2001), allow for highly efficient polarization transfer but are limited to the observation of one- or two-bond proximities due to their sensitivity to dipolar truncation (Bayro et al. 2009; Ladizhansky 2009). Dipolar truncation helps in the selective assignment of ^{13}C backbone structure but does not yield information on sidechain correlations. The proton-assisted spin diffusion (2nd-order recoupling) methods, such as PDSD (Szeverenyi et al. 1982), DARR (Takegoshi et al. 2001), RAD (Morcombe et al. 2004), MIRROR (Scholz et al. 2008), PARIS (Weingarth et al. 2009), RDSD (Hou et al. 2011), SHANGHAI (Hu et al. 2011) and their variants, are broadbanded and less sensitive to dipolar truncation. Therefore, these sequences permit the observation of sufficient number of long-range ^{13}C–^{13}C correlations in U-^{13}C-labled proteins with long recoupling times and low radio frequency (RF) fields, which is essential for the 3D structure determination in proteins. Among these methods, recoupling schemes such as PARIS$_{xy}$ (Weingarth et al. 2010), SHANGHAI+ (Hu et al. 2012), are found to be more broadbanded and efficient compared with other sequences. Recently, we have developed a 2nd-order recoupling scheme named CORD (COmbined $R2^{v}_{n}$-Driven recoupling, Fig. 1b) based on a series of modified $R2^{v}_{n}$-Driven Spin Diffusion sequences, and have demonstrated that CORD exhibits high transfer efficiency and broadband excitation for both aliphatic-to-aliphatic and aliphatic-to-carbonyl carbon regions at fast MAS (Hou et al. 2013).

In this work, we present a family of experiments that combine fpRFDR$_{xy16}$ and CORD$_{xy4}$ schemes during the mixing period (Fig. 1), to exploit the advantages of both techniques and attain highly efficient dipolar recoupling for both short- and long-range correlations in the same measurement. CORD–RFDR sequences yield long-range cross peaks and give rise to enhanced cross peak intensities across the entire correlation spectrum. We have verified this behavior experimentally and by numerical simulations on U-^{13}C,^{15}N-MLF tripeptide. We present the analysis of the empirically derived distance-dependent polarization transfer dynamics. We demonstrate the applications of 2D CORD–RFDR correlation spectroscopy in an 89-residue dynein light chain LC8 and in tubular assemblies of HIV-1 CA protein. On the basis of our results we conclude that CORD–RFDR experiment is beneficial for homonuclear correlation spectroscopy in a broad range of conditions, including both moderate and high magnetic fields and MAS frequencies.

Experiments and methods

Materials

U-^{13}C,^{15}N-Met-Leu-Phe (MLF) tripeptide was purchased from Cambridge Isotope Laboratories and used without any further purification or re-crystallization. MLF powder sample was packed into a 1.6 mm Agilent MAS rotor for subsequent NMR experiments at 14.1 T. U-^{13}C,^{15}N-dynein light chain LC8 protein was expressed in *Escherichia coli*, purified, doped with Cu(II)-EDTA to the final concentration of Cu^{2+} of 5 mM, and precipitated by controlled precipitation from PEG-3350, as described previously (Marulanda et al. 2004; Sun et al. 2012b). 9.6 mg of LC8 precipitate were packed into a 1.9 mm Bruker MAS rotor for subsequent NMR experiments at 20.0 T. Expression and purification of HIV-1 CA (NL4-3 A92E construct) were performed as reported previously (Han et al. 2013). Tubular assemblies of CA were prepared from 32 mg/mL protein solutions in 25 mM phosphate buffer (pH 5.5) containing 1 M NaCl. 25.8 mg of CA tubular assemblies

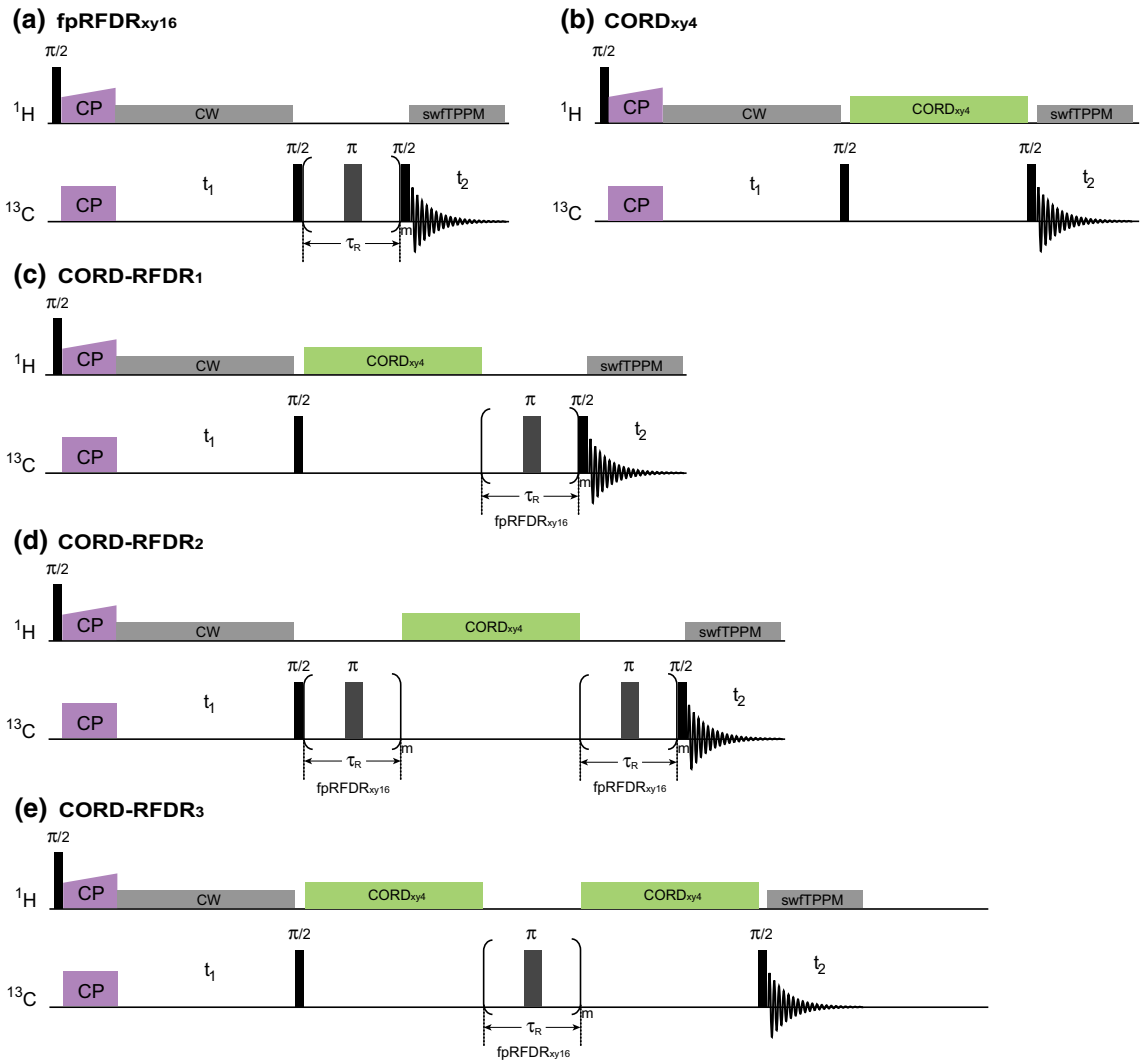

Fig. 1 Pulse sequences for the following 2D experiments: **a** fpRFDR$_{xy16}$, **b** CORD$_{xy4}$, and **c**–**e** CORD–RFDR and its variants. The CORD$_{xy4}$ irradiation scheme is composed of rotor-synchronized $R2^{v}_{n}$-type symmetry-based sequences ($R2^{1}_{1}$, $R2^{2}_{1}$, $R2^{1}_{2}$, $R2^{2}_{2}$), supercycled by XY4 phase cycle (xy-x-y). The fpRFDR$_{xy16}$ sequence employs the XY16 phase cycle (xyxy yxyx -x-y-x-y -y-x-y-x). For recording long-range correlations, the CORD–RFDR scheme combines CORD$_{xy4}$ executed with long mixing times (200–500 ms) and fpRFDR$_{xy16}$ elements placed at different positions

were packed into a 3.2 mm Bruker MAS rotor for subsequent NMR experiments at 20.0 T.

NMR spectroscopy

Experiments were conducted on a 14.1 T Varian Infinity-Plus and a 20.0 T Bruker AVANCE III standard bore NMR spectrometers, with ^{1}H and ^{13}C Larmor frequencies of 599.8/850.4 and 150.8/213.8 MHz, respectively. A 1.6 mm triple-resonance Varian HXY MAS probe was used for the experiments performed at 14.1 T on MLF sample, and all spectra were recorded at the MAS frequency of 40 kHz, controlled to within ±5 Hz using a Varian MAS controller. The typical 90-degree pulse lengths were 2 μs (^{1}H) and 3 μs (^{13}C). A Bruker 1.9 mm and a Bruker 3.2 mm triple-resonance HCN MAS probes were used for the experiments on LC8 and HIV-1 CA samples at 20.0 T, respectively. The MAS frequency was 40 and 14 kHz for experiments of LC8 and HIV-1 CA, respectively, and controlled to within ± 5 Hz using a Bruker MAS controller. The typical 90-degree pulse lengths were 1.7 μs (^{1}H) and 2.5 μs (^{13}C).

To reduce sample heating during MAS, nitrogen gas was used for cooling, resulting in a final sample temperature of 4 °C for LC8 and HIV-1 CA, and 20 °C for MLF. Low-power TPPM ^{1}H decoupling with the RF field strength of 10 kHz was used during the t_1 and t_2 periods at MAS frequency of 40 kHz. High-power SPINAL ^{1}H decoupling

with the RF field strength of 80 kHz was used during the t_1 and t_2 periods at MAS frequency of 14 kHz. No decoupling was applied during the fpRFDR mixing periods at MAS frequency of 40 kHz. The ^1H–^{13}C cross polarization was performed with a linear amplitude ramp (90–110 %) on ^{13}C, the center of the ramp Hartmann–Hahn matched to the first spinning sideband. During the mixing period, different composite pulse irradiations were applied, and a series of corresponding 2D NMR spectra were recorded. The RF fields on the ^1H channel during the CORD mixing time were set to $\nu_{1H} = \nu_R$ and $\nu_R/2$ for $R2_1^\nu$ and $R2_2^\nu$ symmetry sequences, respectively. RF field strengths of 80 kHz on the ^{13}C channel were used for $fpRFDR_{xy16}$ sequences. All 2D NMR data were processed with NMRPipe (Delaglio et al. 1995) in a Mac environment using a standard protocol including apodization, Fourier transform, phase correction and baseline correction in both dimensions. Additional relevant experimental and processing parameters are specified in the supporting information Table S1.

Numerical simulations

All numerical simulations were performed using SIMPSON (Bak et al. 2000). 168 REPULSION angles (α, β) and 13 γ angles were used to generate a powder average. The atomic coordinates for the model spin systems employed in the simulations were taken from the SSNMR structure of the leucine residue in the N-f-MLF-OH tripeptide (PDB ID 1Q7O) (Rienstra et al. 2002). The one-bond dipolar coupling constants for ^1H–^{13}C and ^{13}C–^{13}C were set as 24,049 and 2,113 Hz, respectively. Throughout the simulations, all possible pairwise dipolar couplings were taken into account. *J*-couplings were ignored since their effects are negligible given their small sizes. Other parameters used in simulations were the same as in the corresponding experiments.

Results and discussion

Polarization transfer efficiencies, excitation bandwidth, short- and long-range correlations

The pulse sequences for the 2D fpRFDR (Brinkmann et al. 2002), CORD (Hou et al. 2013) and CORD–RFDR experiments are shown in Fig. 1. fpRFDR is an efficient zero-quantum dipolar correlation method, especially at fast MAS frequencies. It consists of a train of π-pulses of finite duration, applied every rotor period on the ^{13}C channel. The XY16 symmetry phase cycle is used to suppress the isotropic chemical shifts, chemical shift anisotropy (CSA) and heteronuclear *J*-couplings. However, the deleterious effects of multi-spin interactions interfere with the efficiency and analysis of fpRFDR in uniformly labeled samples. In particular, the recoupling of a small dipolar coupling between a distant spin pair is severely attenuated in the presence of a third spin strongly coupled to either of the two spins, the so-called dipolar truncation effect (Bayro et al. 2009), prohibiting the measurement of long-range distances, which are important in constraining structures. The second-order recoupling sequences, such as $CORD_{xy4}$ developed by us recently, does not suffer from dipolar truncation (Hou et al. 2013). CORD sequence is comprised of four $R2_n^\nu$ sequences ($R2_1^1$, $R2_1^2$, $R2_2^1$, $R2_2^2$), whose combination produces truly broadbanded ^{13}C–^{13}C spin diffusion with efficient polarization transfer across the entire spectral range. However, CORD requires the presence of protons and is not applicable to the perdeuterated proteins. Furthermore, its efficiency is inversely proportional to the MAS frequency, which leads to the reduction in polarization transfer efficiency at MAS frequencies of 40 kHz and higher.

In our attempt to overcome the above problems of dipolar truncation and MAS frequency dependence of polarization transfer efficiency in a single experiment, we have explored the family of CORD–RFDR experiments, where $fpRFDR_{xy16}$ and $CORD_{xy4}$ schemes are combined during the mixing time. We have designed different types of CORD–RFDR combinations (Fig. 1c–e) and assessed their performance experimentally (Fig. 3c–e). The results indicate that the combined CORD–RFDR experiments retain the useful features of both $fpRFDR_{xy16}$ and $CORD_{xy4}$: they exhibit higher transfer efficiencies than $CORD_{xy4}$, do not suffer from dipolar truncation like $fpRFDR_{xy16}$, and provide broadband recoupling across the entire chemical shift range. As shown below, the performance of the various CORD–RFDR variants is similar, and therefore, as the default sequence we will discuss the CORD–$RFDR_2$ (Fig. 1d), except where indicated explicitly.

To examine the properties of the above sequences at $\nu_R = 40$ kHz, we have performed numerical simulations of the polarization transfer efficiencies in a C_2H_2 spin model as a function of the chemical shift (resonance frequency) difference and RF power, for each recoupling scheme. As shown in Fig. 2a, the $fpRFDR_{xy16}$ sequence exhibits uniformly high transfer efficiencies across the entire spectrum when the RF power exceeds 100 kHz. When the RF power is below 80 kHz, the transfer efficiencies are lower and strongly dependent on the chemical shift difference. We also note that these generally high polarization transfer efficiencies predicted by numerical simulations are in practice tampered by relatively short signal decays, resulting in severe signal attenuation (Hou et al. 2013).

For the $CORD_{xy4}$ sequences, polarization transfers are broadbanded over a wide range of RF powers, as illustrated

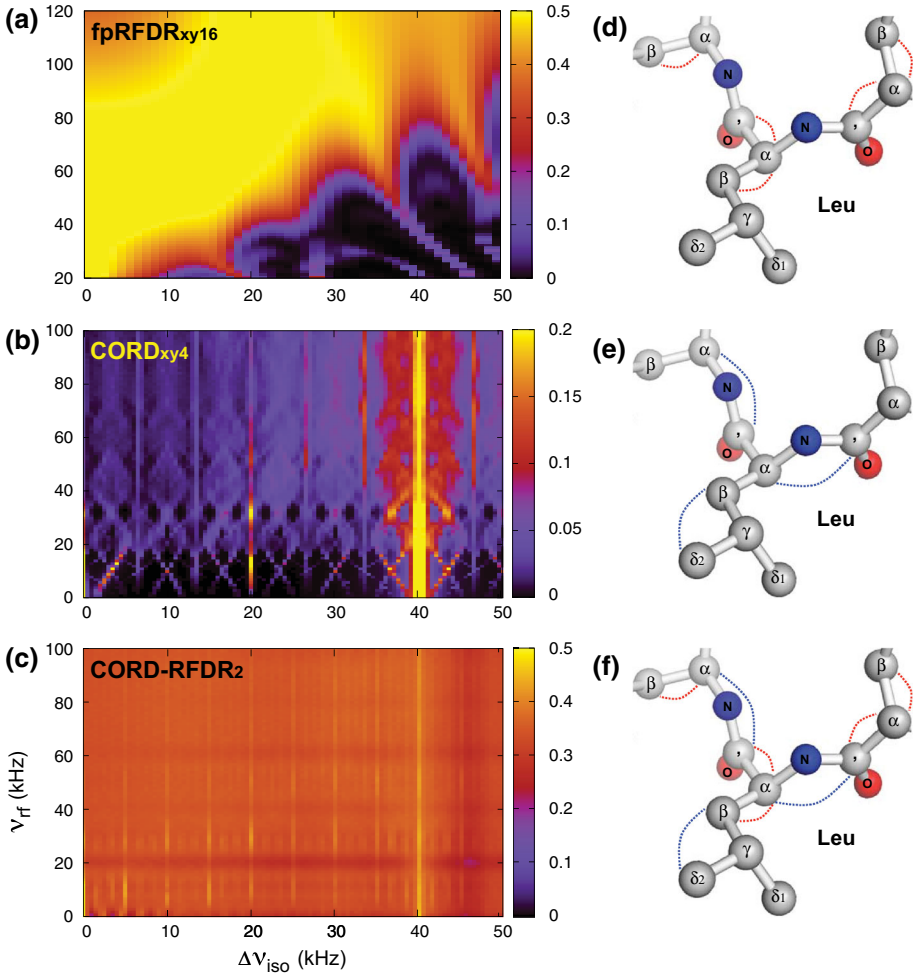

Fig. 2 Simulated dependencies of ^{13}C–^{13}C polarization transfer efficiencies on RF field strength and the resonance frequency difference, for the following experiments: **a** fpRFDR$_{xy16}$, **b** CORD$_{xy4}$, and **c** CORD–RFDR. A C_2H_2 spin model was used for the simulations; the MAS frequency was 40 kHz and the magnetic field strength 14.1 T. The fpRFDR and CORD mixing times were 2.4 and 150 ms, respectively. The *colored dashed lines* in (**d**–**f**) indicate the polarization transfer pathways operational in U-^{13}C,^{15}N-MLF tripeptide during each experiment

in Fig. 2b and in our recent report (Hou et al. 2013). The vertical axis represents RF powers for $R2_1^v$-type symmetry-based sequences in CORD $_{xy4}$, and the RF powers for $R2_2^v$ sequences were kept as half of those for $R2_1^v$ sequences. The polarization transfer in these experiments is driven by the broadened 2nd-order rotational resonance condition $(\nu_{rf} \pm n\nu_R - K_{sc}\nu_{DD} \leq \nu_{iso} \leq \nu_{rf} \pm n\nu_R + K_{sc}\nu_{DD}$, where $K_{sc}\nu_{DD}$ denotes the scaled effective dipolar couplings reintroduced by $R2_n^v$ symmetry sequences, and ν_{DD} is the ^1H–^{13}C dipolar coupling constant), with various recoupling sequences applied on the protons. The combination of different $R2_n^v$-based elements leads to a broadband excitation with the entire ^{13}C ν_{iso} range. The simulated transfer efficiencies are generally lower than for the fpRFDR$_{xy16}$ mixing. However, in practice in organic and biological solids the experimentally attained transfer efficiencies are considerably higher than the simulated ones because of dense ^1H–^1H networks (Hou et al. 2011, 2013; Hu et al. 2011, 2012; Ladizhansky 2009; Weingarth et al. 2009). Multiple ^1H–^1H dipolar couplings and appreciable ^1H CSA can significantly enhance the transfer efficiencies in these $R2_n^v$-based spin diffusion experiments (Hou et al. 2011). Most importantly, with CORD sequences long-range ^{13}C–^{13}C correlations in U-^{13}C labeled samples are efficiently recorded, as reported by us previously (Hou et al. 2013).

The limitations of the individual fpRFDR and CORD sequences are circumvented in the combined CORD–RFDR experiment. As illustrated in Fig. 2c, the CORD–RFDR mixing gives rise to uniformly high and broadband polarization transfers, which are independent of the RF power employed during the combined mixing period. In these simulations, we fixed the RF power of fpRFDR$_{xy16}$ at 80 kHz on the ^{13}C channel and optimized the recoupling power of CORD$_{xy4}$ on the ^1H channel. The effective polarization transfer was found to be determined by the averaged transfer distribution, where the polarization transfer efficiencies were improved and the bandwidth was increased with respect to the individual fpRFDR$_{xy16}$ and CORD$_{xy4}$ experiments. The two periods of fpRFDR$_{xy16}$ recoupling can be thought to work as bridges by extending the proton-assisted polarization transfer of CORD$_{xy4}$ to nuclei more distant than those in the individual fpRFDR$_{xy16}$ or CORD$_{xy4}$ methods while also enhancing

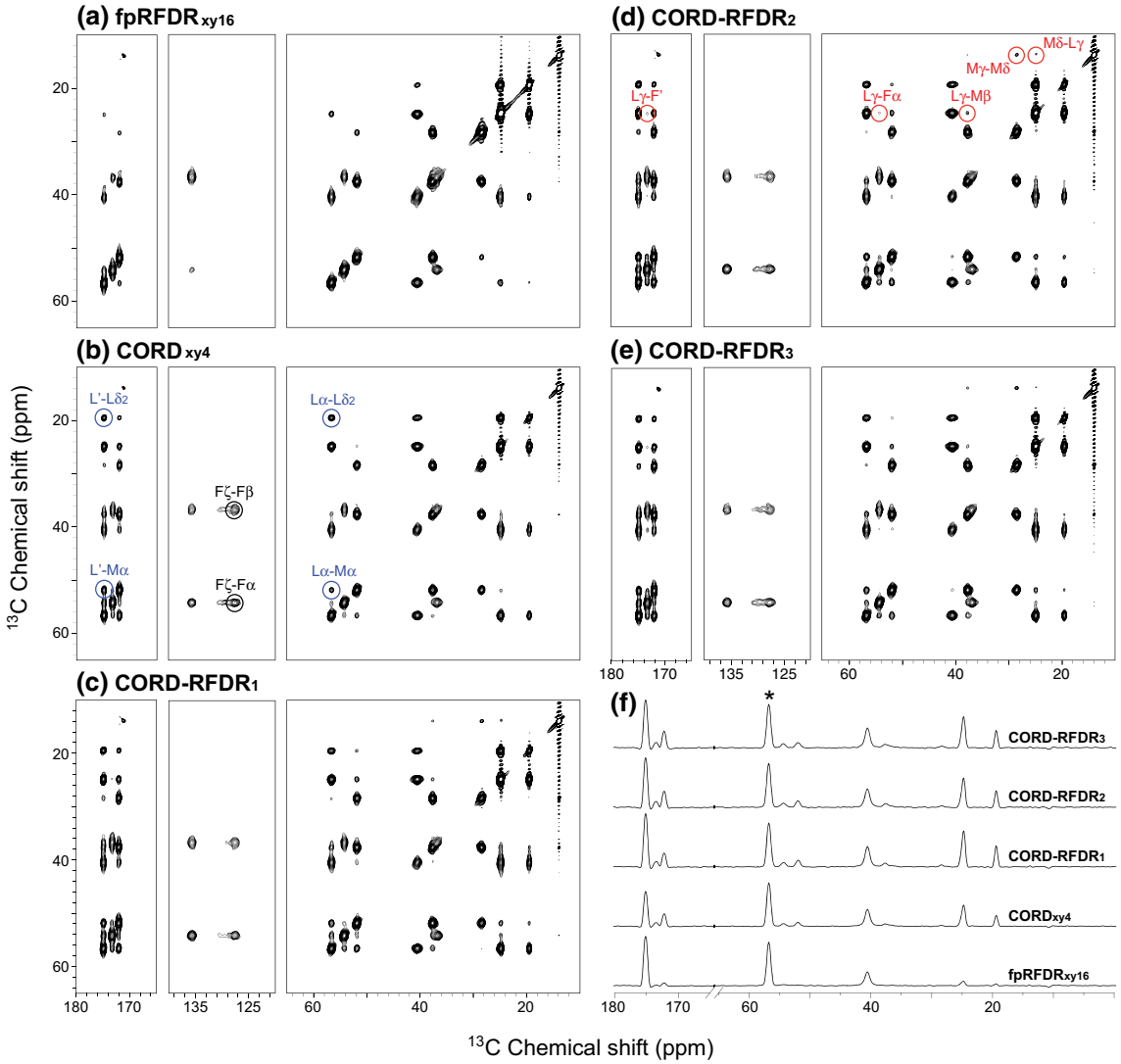

Fig. 3 2D ^{13}C–^{13}C correlation NMR spectra of U-^{13}C,^{15}N-MLF tripeptide acquired with the following mixing sequences: **a** fpRFDR$_{xy16}$, **b** CORD$_{xy4}$, and **c**–**e** CORD–RFDR and its variants. **f** Comparison of the 1D traces extracted along the t_2 dimension of the 2D spectra; the intensity was normalized to the Leu-Cα diagonal peak at 56.7 ppm. The spectra were recorded at the MAS frequency of 40 kHz and magnetic field of 14.1 T. The mixing times were 2.4, 500, 500/2.4, 1.2/500/1.2, and 250/2.4/250 ms respectively

the transfer efficiencies between nuclei separated by shorter distances. This combined mixing scheme creates a more complex averaged polarization transfer network and takes advantage of the high efficiencies provided by fpRFDR$_{xy16}$ with short mixing time. Furthermore, results in Fig. 2c indicate that it is possible to obtain transfer efficiencies at low ^{1}H RF recoupling fields (5–20 kHz) that are as high as those attained with moderate and high RF fields, which is very useful for preventing heating in biological samples.

The experimental results are fully consistent with the above predictions made on the basis of the numerical simulations. In Fig. 3, fpRFDR$_{xy16}$, CORD$_{xy4}$ and CORD–RFDR 2D ^{13}C–^{13}C correlation spectra are displayed; the contour plots are generated with identical contour levels and signal-to-noise ratio (SNR). As anticipated, the CORD–RFDR spectra exhibit both fully broadband excitation and high polarization transfer efficiency for cross peaks. The polarization transfer efficiencies for one-bond cross peaks are somewhat lower than those in the fpRFDR$_{xy16}$ sequence; however, in the latter case high transfer efficiencies are found for both uninformative diagonal peaks and informative cross peaks. Furthermore, the optimal fpRFDR recoupling time giving rise to the most intense peaks in the spectra is 2.4 ms, and under these conditions predominantly one-bond correlations are present. At longer mixing times, rapid deterioration of signal intensities is observed, caused by polarization decay due to the existence of residual ^{1}H–^{13}C and multiple ^{13}C–^{13}C dipolar couplings of similar magnitudes. This behavior

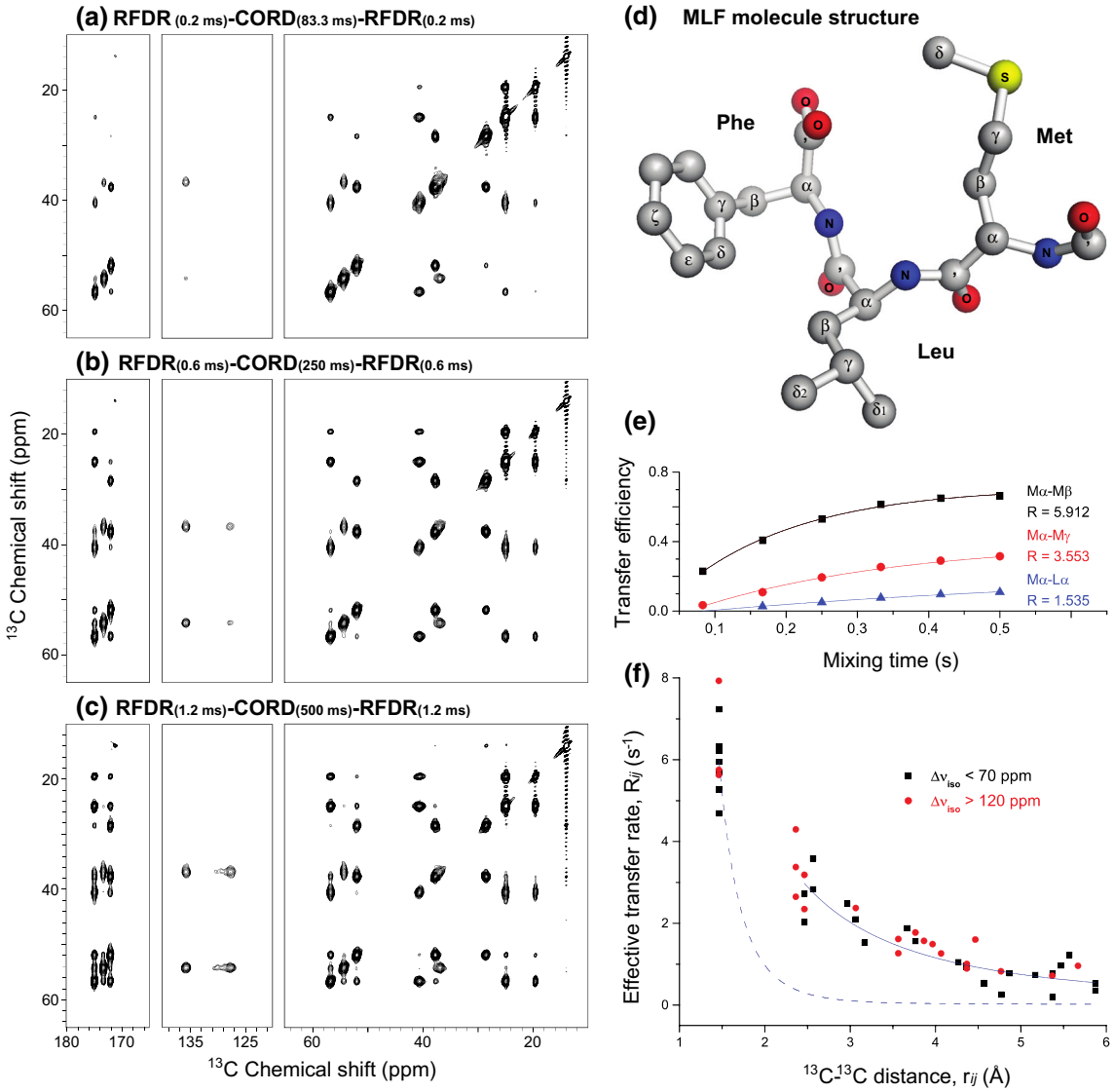

Fig. 4 **a–c** 14.1 T 2D ^{13}C–^{13}C CORD–RFDR correlation NMR spectra of U-^{13}C,^{15}N-MLF tripeptide acquired with different $fpRFDR_{xy16}$ and $CORD_{xy4}$ mixing times. The MAS frequency was 40 kHz. **d** Molecular structure of MLF. **e** The transfer efficiencies for three representative ^{13}C spin pairs plotted as a function of the mixing time. The transfer efficiency is defined as the ratio of twice the integrated intensity of the cross peak to the sum of integrated intensities of the corresponding diagonal peaks. **f** Effective polarization transfer rates plotted as a function of ^{13}C–^{13}C distances, from experimental CORD–RFDR data on MLF presented in Table 1. Effective polarization transfer rates for ^{13}C–^{13}C spin pairs with small and large chemical shifts difference are represented in *black squares* and *red dots*, respectively. A reference fitting for zero-quantum recoupling exhibiting the relationship $R_{ij} \propto r_{ij}^{-6}$ is plotted as *blue dashed curve*. The empirical fitting of the experimental data to $R_{ij} \propto r_{ij}^{-2}$ is plotted as *solid blue curve*, and corresponds to the contribution from the proton-assisted spin diffusion

makes fpRFDR experiments with long mixing times inefficient. As discussed above, dipolar truncation precludes recording long-distance correlations in fpRFDR.

In contrast to fpRFDR, in the $CORD_{xy4}$ experiment acquired with the mixing time of 500 ms, one could easily detect three-bond correlations between aliphatic sites (such as Lα–Lδ$_2$, Lα–Mα) as well as four-bond correlations between aliphatic and carbonyl atoms (such as L′–Lδ$_2$, L′–Mα) and those within the aromatic sidechain atoms (such as Fζ–Fβ, Fζ–Fα).

In the CORD–RFDR experiment, the polarization transfer network is further extended yielding correlations between atoms separated by five and six bonds (such as Lγ–F′, Lγ–Fα, Lγ–Mβ), see Fig. 3d. The most distant spin pairs in the MLF molecule (such as Mδ–Lγ, related to 7–9 Å) can also be detected. Furthermore, the spectra reveal that the efficiencies of polarization transfers between proximal atoms (such as Mγ–Mδ) are considerably enhanced. These conclusions apply to all variants of CORD–RFDR sequence presented in Fig. 1, as illustrated

in Fig. 3c–e. Figure 3f displays the comparison of 1D traces extracted along the t_2 dimension of the individual 2D spectra. It is clear that the transfer efficiencies in both aliphatic and carbonyl regions, for both short- and long-range correlations are considerably improved in the CORD–RFDR sequences vis-à-vis the corresponding CORD and fpRFDR experiments.

Analysis of distance dependence of polarization transfer efficiency

To understand the contributions to the polarization buildup dynamics arising from the individual $fpRFDR_{xy16}$ and $CORD_{xy4}$ mixing elements to the combined CORD–RFDR experiment, we collected a series of CORD–$RFDR_2$ spectra of U-^{13}C,^{15}N MLF trepeptide at the MAS frequency of 40 kHz. In these experiments, the RFDR/CORD/RFDR mixing times were 0.2/83/0.2, 0.4/167/0.4, 0.6/250/0.6, 0.8/333/0.8, 1.0/417/1.0, and 1.2/500/1.2 ms. These mixing time combinations were chosen on the basis of the experimentally optimized mixing times of 2.4 and 500 ms for the individual $fpRFDR_{xy16}$ and $CORD_{xy4}$ experiments, respectively. In this series of data, we have investigated the polarization transfer efficiencies for short- and long-range ^{13}C–^{13}C correlations. As summarized in Fig. 4, as the mixing time is increased, longer-range cross peaks become prominent in the spectra, and we detected correlations corresponding to ^{13}C–^{13}C distances as long as 7–9 Å (corresponding to atoms separated by 7–8 bonds in the MLF structure).

Analysis of the polarization transfer dynamics of various cross peaks in the spectra reveals that the intensities of one-bond cross peaks decay as the mixing times are increased, while those of the medium- and long-range cross peaks grow monotonously as a function of the mixing time. This result suggests that medium- and long-range polarization transfers originate predominantly from the proton-assisted spin diffusion during the $CORD_{xy4}$ periods. Because of dipolar truncation, medium- and long-range transfers cannot be realized during the $fpRFDR_{xy16}$ mixing period, and $fpRFDR_{xy16}$ may instead facilitate, through short-range ^{13}C–^{13}C and ^{13}C–^{1}H transfers, establishing a more uniform average transfer network amongst all the possible ^{13}C nuclei.

As reported elsewhere (Dumez and Emsley 2011; Hou et al. 2006; Luo and Hong 2006), the polarization transfer between the coupled spin pairs in the spin-diffusion type experiments can approximately be described by the constant transfer rate, k_{ij}, which mostly depends on the internuclear distance and the abundant proton bath. The polarization transfer buildup curves for representative ^{13}C–^{13}C spin pairs of MLF in CORD–RFDR experiments are illustrated in Fig. 4e. As discussed above, in CORD–RFDR the main contribution to the detected ^{13}C–^{13}C correlations (particularly for those between carbons separated by multiple bonds) arises from the proton-assisted spin diffusion portion of the sequences, $CORD_{xy4}$. Therefore, the effective polarization transfer rate R_{ij} between carbon atoms C_i and C_j may be approximated by an exponential relationship between the experimental transfer efficiency and the mixing times. Figure 4e illustrates that the effective transfer rate and the maximum attainable polarization transfer efficiencies are dependent on the $CORD_{xy4}$ mixing time and the interatomic distance between the different spin pairs. We define R as the effective transfer rate, calculated from the buildup curve as the effective rate constant of the exponential buildup/decay. As shown in Fig. 4e, the one-bond Mα–Mβ spin pair has fast buildup and R of 5.912; two-bond Mα–Mγ and three-bond Mα–Lα spin pairs have slower buildup rates and lower R of 3.553

Table 1 Summary of the effective polarization transfer rates

Spin pair	Distance (Å)	R (s^{-1})	Spin pair	Distance (Å)	R (s^{-1})
Short-range					
M′–Mα	1.5	5.714	M′–Mβ	2.4	3.344
Mα–Mβ	1.5	5.912	M′–Lα	2.4	4.261
Mβ–Mγ	1.5	4.656	Mα–Mγ	2.6	3.553
L'–Lα	1.5	5.586	L′–Lβ	2.5	3.152
Lα–Lβ	1.5	6.271	L′–Fα	2.4	2.617
Lβ–Lγ	1.5	5.238	Lα–Lγ	2.6	2.803
Lγ–Lδ2	1.5	6.187	Lβ–Lδ2	2.5	2.7
F′–Fα	1.5	7.883	F′–Fβ	2.5	2.318
Fα–Fβ	1.5	5.656	Fα–Fγ	2.5	2.001
Fβ–Fγ	1.5	7.184			
Medium-range					
M′–Mγ	3.8	1.747	M′–Lγ	4	1.464
M′–L′	3.2	1.495	Mα–L′	4.4	0.981
M′–Lβ	3.6	1.241	Mβ–L′	4.5	1.575
Mα–Lα	3.8	1.535	Mβ–Lα	4.3	1.023
L′–Lγ	3.9	1.542	L′–Lδ2	4.4	0.871
L′–F′	3.7	1.855	L′–Fγ	3.6	1.587
L′–Fβ	3.1	2.343	M′–Lδ2	4.1	1.236
Lα–Lδ2	3	2.445	Lα–Fβ	4.4	0.903
F′–Fγ	3.1	2.069	Lβ–Fα	4.4	0.94
Long-range					
Mγ–Lα	5.5	0.94	Mα–Lδ2	5.2	0.718
Mα–Lβ	4.8	0.231	Mβ–Lγ	5.9	0.5
Mβ–Lβ	5.4	0.166	Mγ–L′	5.7	0.932
Mα–Lγ	4.9	0.75	M′–F′	5.4	0.75
Lα–F′	4.8	0.798	Lγ–Fα	5.9	0.336
Lα–Fγ	4.6	0.514	Fα–Lα	5.6	1.207
Lβ–F′	5.4	0.691			

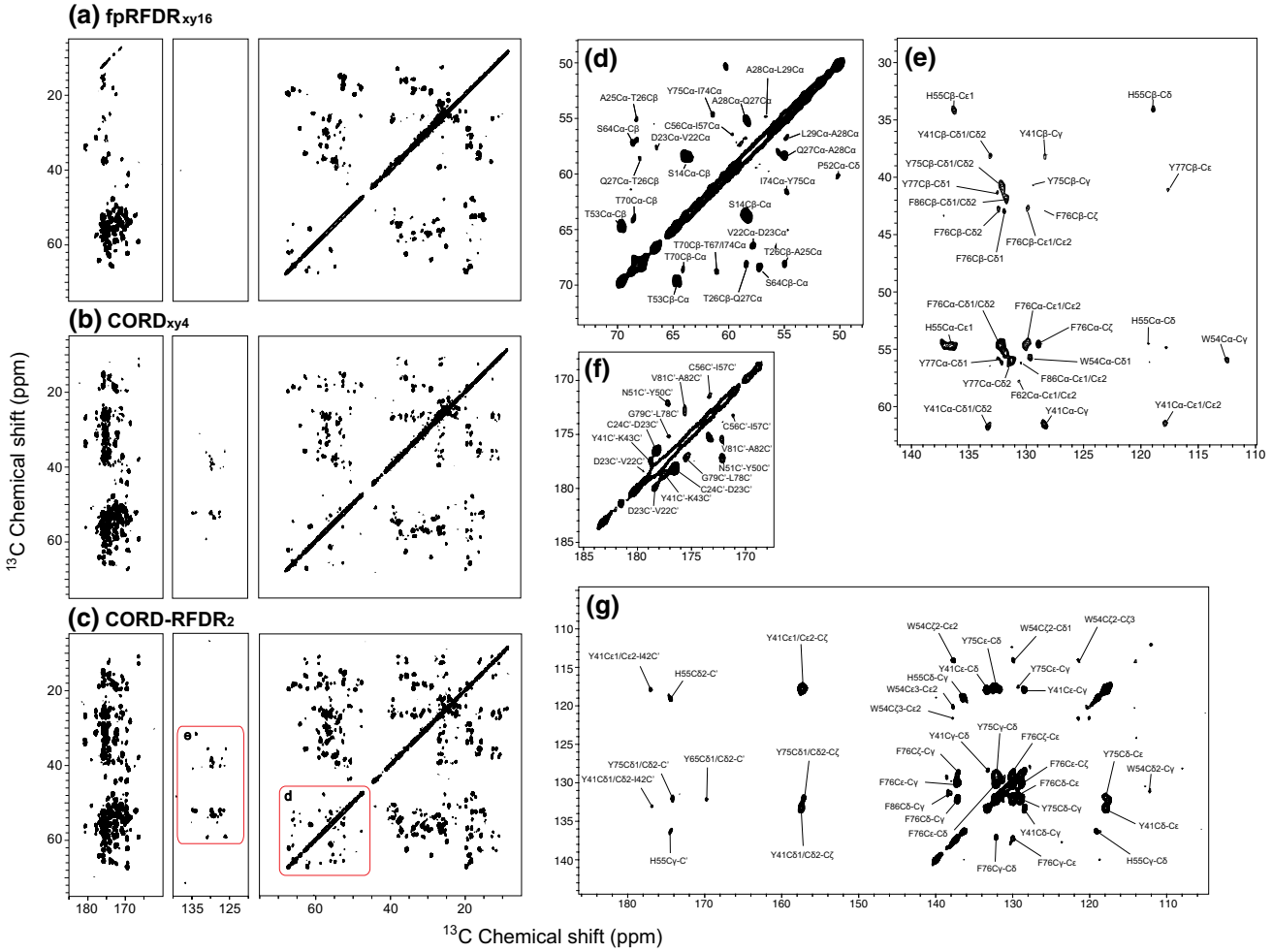

Fig. 5 2D ^{13}C–^{13}C correlation spectra of U-^{13}C,^{15}N-LC8 protein acquired at the magnetic field of 20.0 T and MAS frequency of 40 kHz with **a** fpRFDR$_{xy16}$, **b** CORD$_{xy4}$, and **c** CORD–RFDR. The CORD–RFDR experiment reveals numerous new cross peaks throughout the entire the chemical shift range as compared to fpRFDR$_{xy16}$ and CORD$_{xy4}$. The Cα region of the CORD–RFDR spectrum shows numerous inter-residue correlations and the aromatic region displays multiple intra-residue side-chain correlations not present in either the CORD or fpRFDR spectra. Assignments of new cross peaks in the various regions of CORD–RFDR spectrum are shown in the magnified views of: **d** aliphatic region, **e** aliphatic–aromatic region, **f** carbonyl region, and **g** aromatic–carbonyl region. Most of the carbons for which new cross peaks were observed are separated by 3–5 Å (medium-range distance). Several correlations corresponding to long-range distances have been detected as well. Table 2 summarizes the new correlations detected in the CORD–RFDR spectrum

and 1.535, respectively. This trend corroborates that the effective transfer rate R_{ij} is related to the dipolar interaction between different spin pairs.

Table 1 presents a summary of the effective transfer rates for all the ^{13}C–^{13}C correlations detected in the CORD–RFDR experiment with the MLF sample. In this table, most of the observed ^{13}C–^{13}C correlations (except for several corresponding to the longest distances, such as Mδ–Lγ) are classified as short-, medium- and long-range according to the interatomic distances. We found that, no matter what the ^{13}C chemical shifts are, the C_i–C_j spin pairs separated by the same distance have similar effective polarization transfer rate, R_{ij}. In other words, R_{ij} is independent of the chemical shift difference. Figure 4f shows the effective transfer rates plotted against the ^{13}C–^{13}C distances for all the detected correlations in Table 1. The data points are divided into two classes corresponding to the different chemical shifts difference, $\Delta\delta_{iso}$, and color-coded accordingly. It is clear from the figure that the effective transfer rates are independent of the chemical shift difference thus providing experimental verification to the simulations results presented in Fig. 2c, namely that the transfer efficiency is uniform and the excitation is broad-band across the full chemical shift range in the CORD–RFDR spectra.

As illustrated in Fig. 4f, we found that the effective polarization transfer rates R_{ij} are generally inversely proportional to the ^{13}C–^{13}C distances, r_{ij}. In the combined

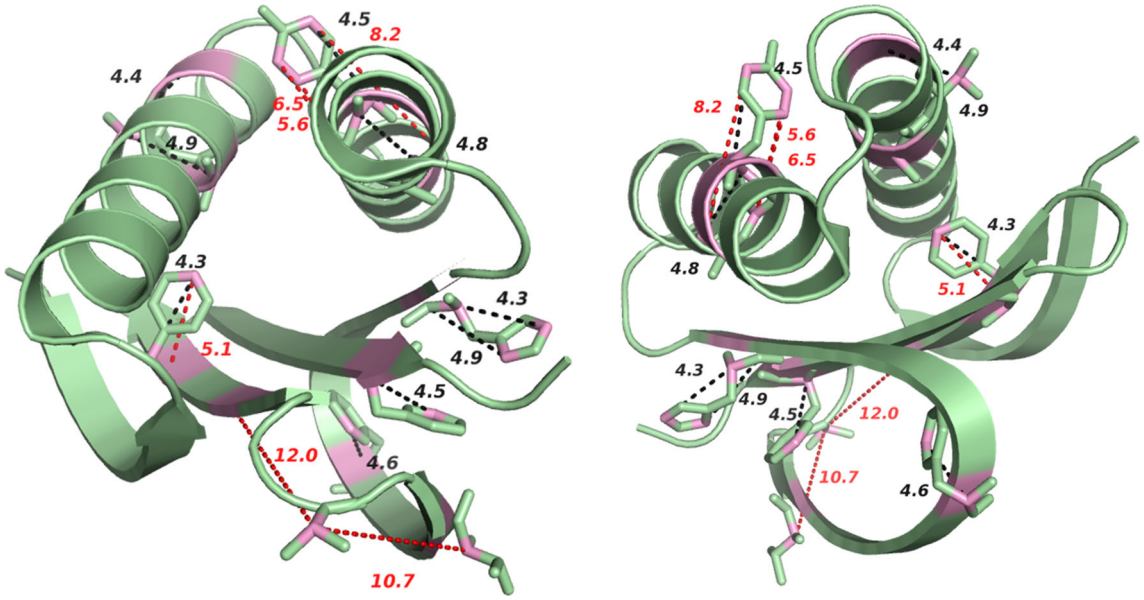

Fig. 6 The representative distance restraints (>4 Å) obtained from CORD–RFDR mapped onto the 3D structure of LC8 (PDB 2PG1) (Williams et al. 2007): top view (*left*), and bottom view (*right*). The atoms among which medium- and long-range correlations were detected in the CORD–RFDR spectrum are shown in *pink*. Distance restraints that are above 5 Å are labeled in *red*

CORD–RFDR scheme, there are two types of distance dependencies that need to be taken into consideration. For the zero-quantum recoupling part, several studies have shown that the effective rate constant k_{ij} for polarization transfer between two ^{13}C atoms is expected to be proportional to the square of the effective dipolar coupling D_{ij} and the inverse 6th power of the distance r_{ij} between these two carbons (Dumez and Emsley 2011; Luo and Hong 2006). As shown in Fig. 4f with the blue dashed line, the effective polarization transfer rate associated with this kind of zero-quantum recoupling decreases very rapidly as the ^{13}C–^{13}C distance increases, which indicates that the zero-quantum recoupling only contributes to the short-range ^{13}C–^{13}C correlations in the combined CORD–RFDR scheme. As illustrated in Fig. 4f with the blue solid line, for spin pairs separated by more than one bond, the effective polarization transfer rates are proportional to the inverse square of the internuclear distance, $R_{ij} \propto r_{ij}^{-2}$; we have derived this dependence empirically by fitting the experimental data. We speculate that this empirically observed dependence of the effective transfer rate on the inverse square of the distance originates predominantly from the 2nd-order proton-assisted spin diffusion part. There are prior reports indicating that the distance dependence of the transfer rates in the spin diffusion experiments is complicated and cannot be described by simple expressions (Dumez and Emsley 2011; Grommek et al. 2006; Veshtort and Griffin 2011). Therefore, full multi-spin numerical simulations are needed to account for the experimental results. We also note that under fast MAS frequencies, the polarization transfer dynamics is affected by the recoupled ^{1}H–^{13}C dipolar, ^{1}H–^{1}H dipolar, ^{1}H CSA and other unsuppressed interactions, which further complicate quantitative distance dependence analysis. Generally, this "$R_{ij} \propto r_{ij}^{-2}$" relationship may vary with the spinning frequency and the spin system (especially proton network) for different samples and experimental conditions, and warrants further experimental and theoretical scrutiny. Such studies are beyond the scope of this work and will be pursued by us separately. Nevertheless, the kind of an ad hoc analysis of effective polarization transfer rates on the internuclear distance presented here might be beneficial for building an empirical distance-based reference for the structural analysis of various kinds of systems.

Applications to proteins

Dynein light chain LC8

To explore the applications of CORD–RFDR to proteins, we have carried out 2D ^{13}C–^{13}C experiments on U-^{13}C,^{15}N-labeled LC8. All spectra were acquired at the magnetic field of 20.0 T and the MAS frequency was 40 kHz (Fig. 5a–c). Interestingly, as shown in Fig. 5, the CORD–RFDR experiment reveals more resolved cross peaks than $CORD_{xy4}$. For instance, the Cα region shows more inter-residue Cα–Cα/Cα–Cβ correlations and the aromatic region displays more intra-residue sidechain correlations for the CORD–RFDR than for the CORD. The intra-residue Cα–Cβ correlations are fully retained in CORD–RFDR. More importantly, the intensities of cross peaks in the different regions of CORD–RFDR are

remarkably offset-independent, in contrast to those in the CORD spectrum. On the basis of the highly informative CORD–RFDR spectrum, we have made unambiguous resonance assignments for LC8. These assignments are in accord with our previous study (Sun et al. 2011), except that we were able to identify and assign additional correlations that were missing in the spectra in our earlier work. The assignments of cross peaks in the aliphatic, aromatic and carbonyl regions of CORD–RFDR spectrum are shown in Fig. 5d–g. In addition to the intra-residue correlations that are readily observed in the CORD spectrum, a number of non-trivial inter-residue cross peaks are worth noting. In the Cα region, we detected both inter-residue Cα–Cα and Cα–Cβ correlations, which we did not observe in any of the spectra collected prior to this study. In the aromatic region, correlations between the Cα/Cβ and aromatic ring carbons may provide the orientational information for the side-chains of the aromatic residues. Most of the correlations in these two regions correspond to atoms that are separated by 3–5 Å, which can be classified as medium-range distances. Longer-range distance correlations are detectable by CORD–RFDR as well, and one such example is the T70Cβ-T67/I74Cα cross peak. There are a total of sixteen assigned long-distance correlations that originate from polarization transfers between i and i ± 1 residues and two assigned correlations associated with more distant residues.

Figure 6 shows the mapping of the representative distance restraints onto the 3D X-ray structure of LC8 protein (PDB 2PG1) (Williams et al. 2007). The distances and distance categories corresponding to the correlations that are only detected by CORD–RFDR experiment are listed in Table 2. Based on the X-ray structure, the distance between T70 Cβ and T67 Cα is about 10.7 Å while the distance between T70 Cβ and I74 Cα is 12.0 Å. The assignment of T70Cβ-T67/I74Cα correlation is ambiguous, yet regardless of whether it corresponds to T67 or I74, the observed distance is in the 10–12 Å range. Correlations corresponding to such long distance are highly unlikely to be observed in the CORD–RFDR spectrum. This suggests three possible scenarios. One is that an intermolecular correlation (crystal packing contacts) is detected. We can neither corroborate nor rule out this possibility because we do not have a crystal structure of LC8 under our NMR conditions. However, the available crystal structure of the LC8 indicates that the closest intermolecular distances between the respective residue pairs are too long (ca. 15–21 Å) to yield CORD–RFDR cross peaks.

The second possibility is that the conformation of the loop containing the T70 residue is different in LC8 prepared for our NMR experiments vis-à-vis the X-ray structure. We speculate that this loop region might reorganize so that T70 becomes positioned close to the T67 and I74 β sheet structures in our NMR sample. Testing this hypothesis requires 3D structure determination of LC8 under our NMR condition; this work is currently ongoing in our laboratory.

The third possibility is that such long-range correlations could arise from multiple shorter-range transfers, due to the net action of the individual RFDR and CORD transfers. Detailed understanding of this effect would require additional experiments (involving dilution of proton spin bath by deuteration) coupled with numerical simulations involving extended proton spin networks. This analysis is

Table 2 Different types of distance restraints revealed by CORD–RFDR in dynein light chain LC8 protein

Restraint name	Distance (Å)	Restraint name	Distance (Å)
Aliphatic–aliphatic			
V22 Cα–D23 Cα	3.8	C56 Cα–I57 Cα	3.8
A25 Cα–T26 Cβ*	4.9	S64 Cα–S64 Cβ	1.5
T26 Cβ–Q27 Cα*	4.4	T70 Cα–T70 Cβ	1.5
Q27 Cα–A28 Cα	3.8	I74 Cα–Y75 Cα	3.8
A28 Cα–L29 Cα	3.8	T67/I74 Cα–T70 Cβ*	10.7/12.0
Aromatic–carbonyl			
Y41 Cε1/Cε2–I42 C′*	7.5/6.5	H55 Cγ–H55 C′	3.8
Y41 Cδ1/Cδ2–I42 C′*	6.8/5.6	Y65 Cδ1/Cδ2–Y65 C′	3.9/3.8
H55 Cδ2–H55 C′*	4.9	Y75 Cδ–Y75 C′	3.7
Carbonyl–carbonyl			
V22 C′–D23 C′	2.9	C56 C′–I57 C′	3.5
D23 C′–C24 C′	3.0	L78 C′–G79 C′	3.0
Y41 C′–K43 C′*	4.8	V81 C′–A82 C′	3.4
Y50 C′–N51C′	3.2		
Aliphatic–aromatic			
A40 Cα–Y41 Cε1/Cε2*	8.2/8.4	F62 Cα–F62 Cε1/Cε2*	4.6/4.7
Y41 Cα–Y41 Cε1/Cε2*	4.5/4.7	Y75 Cβ–Y75 Cδ	2.5
Y41 Cα–Y41 Cδ1/Cδ2	3.3/3.5	Y75 Cβ–Y75 Cγ	1.5
Y41 Cα–Y41 Cγ	2.5	Y77 Cα–Y77 Cδ1	3.3
Y41 Cβ–Y41 Cδ	2.5	Y77 Cβ–Y77 Cε	3.8
Y41 Cβ–Y41 Cγ	1.5	Y77 Cβ–Y77 Cδ1	2.5
W54 Cα–W54 Cδ1	3.4	F76 Cβ–F76 Cδ2	2.5
W54 Cα–W54 Cγ	2.5	F76 Cβ–F76 Cδ1	2.5
W54 Cβ–W54 Cγ	1.5	F76 Cβ–F76 Cε	3.8
H55 Cα–H55 Cε1*	4.3	F76 Cβ–F76 Cζ*	4.3
H55 Cα–H55 Cδ2	3.6	F76 Cα–F76 Cζ*	5.1
H55 Cβ–H55 Cε1	3.6	F86 Cβ–F86 Cδ	2.5
H55 Cβ–H55 Cδ2	2.6	F86 Cα–F86 Cε1/Cε2*	4.5/4.6
Aromatic–aromatic			
W54 Cζ2–W54 Cε3	2.8	Y41 Cγ–Y41 Cδ	1.4
W54 Cζ2–W54 Cδ1	3.6	Y75 Cδ–Y75 Cζ	2.4
W54 Cε2–W54 Cε3	2.4	Y75 Cε–Y75 Cγ	2.4
W54 Cζ3–W54 Cε2	2.7	F86 Cγ–F86 Cδ	1.4
W54 Cγ–W54 Cδ2	1.4		

Restraints labeled with * are mapped onto 3D X-ray structure of LC8 shown in Fig. 6

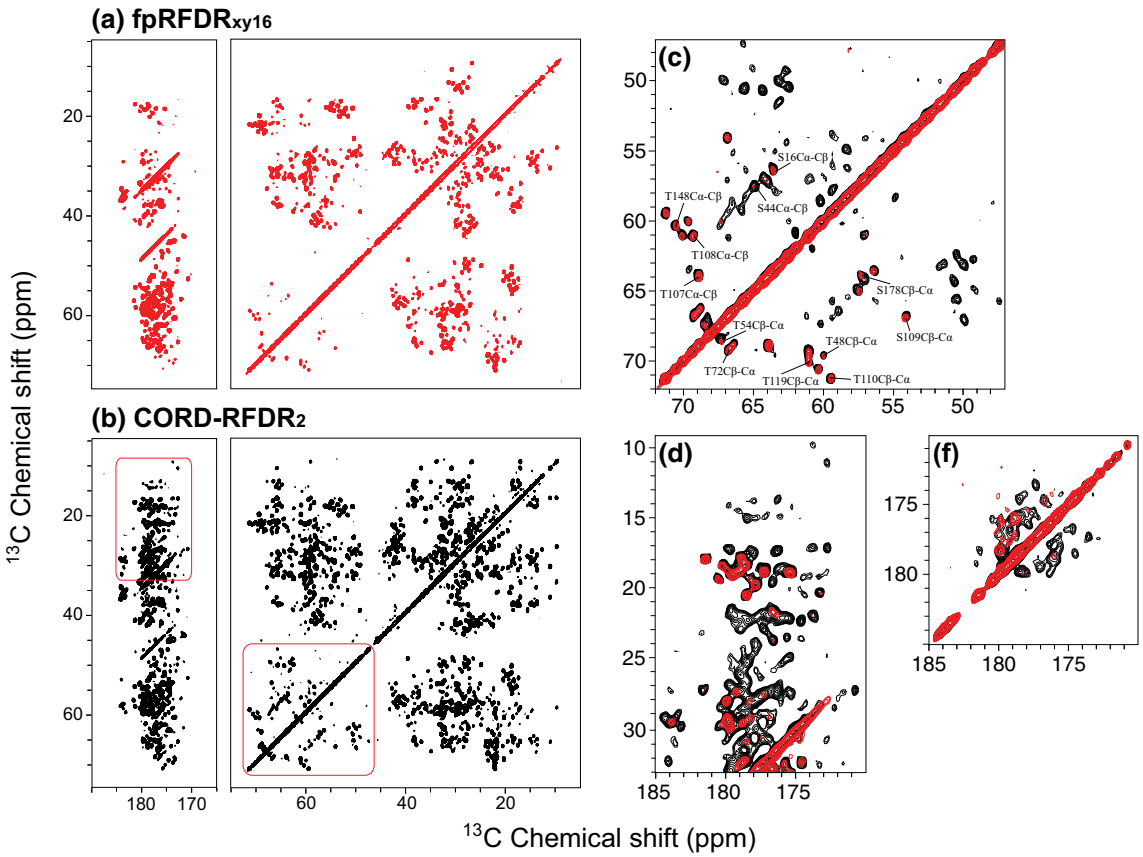

Fig. 7 2D ^{13}C–^{13}C correlation spectra of tubular assemblies of HIV-1 CA protein acquired at the magnetic field of 20.0 T and MAS frequency of 14 kHz with **a** $fpRFDR_{xy16}$, **b** CORD–RFDR, with identical number of scans. The CORD–RFDR experiment reveals numerous new cross peaks throughout the entire the chemical shift range as compared to $fpRFDR_{xy16}$. Representative expansions of enhanced ^{13}C–^{13}C correlation regions by CORD–RFDR: **c** aliphatic region, **d** aliphatic–carbonyl region, and **f** carbonyl region, with $fpRFDR_{xy16}$ (*red*) superimposed on CORD–RFDR (*black*). Assignments of short-range Cα–Cβ correlations in the Ser/Thr region of the spectrum are shown in **c**

beyond the scope of the current article and will be pursued by us in the future.

HIV-1 protein assembly

It is also very interesting to compare the transfer efficiencies of $fpRFDR_{xy16}$, $CORD_{xy4}$ and CORD–RFDR methods in the moderate MAS frequency regime (10–20 kHz). Since the polarization transfer efficiency of CORD scheme is inversely proportional to the spinning frequency, the efficiency of $CORD_{xy4}$ and CORD–RFDR experiments is expected to increase as the MAS frequency decreases. With the HIV-1 CA tubular assemblies, we performed ^{13}C–^{13}C $fpRFDR_{xy16}$, $CORD_{xy4}$ and CORD–RFDR 2D experiments at the MAS frequency of 14 kHz, where high power ^{1}H decoupling was applied during the fpRFDR periods to suppress ^{1}H–^{13}C heteronuclear dipolar couplings. Figure 7 shows the 2D ^{13}C–^{13}C correlation spectra acquired with $fpRFDR_{xy16}$ and CORD–RFDR methods. As illustrated, across the entire spectral range, we have observed many more cross peaks and considerably higher transfer efficiencies for both short- and long-range ^{13}C–^{13}C correlations in the CORD–RFDR compared to $fpRFDR_{xy16}$ spectra. Particularly important are the new or enhanced long-range inter-residue Cα–Cα and C′–C′ correlations that play a critical role in the resonance assignments and constraining the 3D structure, as discussed above for the LC8. Figure 7c–e illustrates representative expansions of enhanced ^{13}C–^{13}C correlation regions by CORD–RFDR. The short-range ^{13}C–^{13}C correlations can be easily detected by both $fpRFDR_{xy16}$ and CORD–RFDR sequences at moderate MAS conditions. On the other hand, numerous additional cross peaks are observed in the CORD–RFDR experiment. These cross peaks likely correspond to medium- and long-range intra- and inter-residue ^{13}C–^{13}C correlations (such as Cα–Cγ, C′–Cβ, Cα–Cα). The comparison of $CORD_{xy4}$ and CORD–RFDR spectra is shown as Figure S1 in the supporting information. This comparison reveals that $CORD_{xy4}$ spectrum acquired with the same number of scans as CORD–RFDR exhibits

considerably higher SNR because it does not suffer from the sensitivity loss due to the fast T_2^{RF} decay during the fpRFDR periods. At the same time, slightly higher transfer efficiencies for cross peaks are observed in the CORD–RFDR, when the CORD–RFDR spectrum is acquired with the number of scans necessary to reach the same sensitivity as the CORD experiment (see the corresponding overlay of the ^{13}C–^{13}C correlation spectra in the supporting information). Under these conditions, CORD–RFDR spectrum exhibits new cross peaks that are missing in the CORD spectrum, including aliphatic-to-aliphatic and aliphatic-to-carbonyl correlations that provide useful structural constraints.

Taken together, our results indicate that CORD–RFDR method is highly advantageous at fast MAS conditions compared to the conventional homonuclear correlation spectroscopy, and could also be useful at moderate MAS frequencies for observing medium- and long-range correlations albeit with somewhat lower sensitivity compared to CORD.

Conclusions

We have demonstrated that combined CORD–RFDR mixing is advantageous for homonuclear correlation spectroscopy in a broad range of MAS frequencies, particularly under fast MAS conditions. CORD–RFDR sequence exhibits uniform and high polarization transfer efficiencies across the entire correlation spectrum and yields long-range cross peaks. Analysis of polarization transfer dynamics revealed an empirical dependence on distance, which is expected to be useful for analysis of distance restraints for protein structure calculations. CORD–RFDR is thus as an efficient broadband dipolar recoupling technique for resonance assignments and structural characterization of biological and organic systems by MAS NMR.

Acknowledgments This work was supported by the National Institutes of Health (NIH Grants P50GM082251, R01GM085306, from NIGMS). We acknowledge the support of the National Science Foundation (NSF Grant CHE0959496) for the acquisition of the 850 MHz NMR spectrometer at the University of Delaware and the National Institutes of Health (NIH Grants P30GM103519 and P30GM110758) for the support of Core Instrumentation infrastructure at the University of Delaware.

References

Bak M, Rasmussen JT, Nielsen NC (2000) SIMPSON: a general simulation program for solid-state NMR spectroscopy. J Magn Reson 147(2):296–330

Bayro MJ, Huber M, Ramachandran R, Davenport TC, Meier BH, Ernst M, Griffin RG (2009) Dipolar truncation in magic-angle spinning NMR recoupling experiments. J Chem Phys 130:114506

Bennett AE, Ok JH, Griffin RG, Vega S (1992) Chemical shift correlation spectroscopy in rotating solids: radio frequency-driven dipolar recoupling and longitudinal exchange. J Chem Phys 96(11):8624–8627

Brinkmann A, Gunne JSAD, Levitt MH (2002) Homonuclear zero-quantum recoupling in fast magic-angle spinning nuclear magnetic resonance. J Magn Reson 156(1):79–96

Delaglio F, Grzesiek S, Vuister GW, Zhu G, Pfeifer J, Bax A (1995) NMRPipe: a multidimensional spectral processing system based on Unix Pipes. J Biomol NMR 6(3):277–293

Dumez JN, Emsley L (2011) A master-equation approach to the description of proton-driven spin diffusion from crystal geometry using simulated zero-quantum lineshapes. Phys Chem Chem Phys 13(16):7363–7370

Ernst M, Meier MA, Tuherm T, Samoson A, Meier BH (2004) Low-power high-resolution solid-state NMR of peptides and proteins. J Am Chem Soc 126(15):4764–4765

Grommek A, Meier BH, Ernst M (2006) Distance information from proton-driven spin diffusion under MAS. Chem Phys Lett 427(4–6):404–409

Han Y, Hou GJ, Suiter CL, Ahn J, Byeon IJL, Lipton AS, Burton S, Hung I, Gor'kov PL, Gan ZH, Brey W, Rice D, Gronenborn AM, Polenova T (2013) Magic angle spinning NMR reveals sequence-dependent structural plasticity, dynamics, and the spacer peptide 1 conformation in HIV-1 capsid protein assemblies. J Am Chem Soc 135(47):17793–17803

Hou GJ, Deng F, Ye CH, Ding SW (2006) Towards uniform enhancement in solid-state cross polarization magnetic angle spinning NMR: a scheme incorporating cross polarization with rotational resonance. J Chem Phys 124:234512

Hou GJ, Yan S, Sun SJ, Han Y, Byeon IJL, Ahn J, Concel J, Samoson A, Gronenborn AM, Polenova T (2011) Spin diffusion driven by R-symmetry sequences: applications to homonuclear correlation spectroscopy in MAS NMR of biological and organic solids. J Am Chem Soc 133(11):3943–3953

Hou GJ, Yan S, Trebosc J, Amoureux JP, Polenova T (2013) Broadband homonuclear correlation spectroscopy driven by combined $R2_n^v$ sequences under fast magic angle spinning for NMR structural analysis of organic and biological solids. J Magn Reson 232:18–30

Hu BW, Lafon O, Trebosc J, Chen Q, Amoureux JP (2011) Broad-band homo-nuclear correlations assisted by H-1 irradiation for bio-molecules in very high magnetic field at fast and ultra-fast MAS frequencies. J Magn Reson 212(2):320–329

Hu BW, Trebosc J, Lafon O, Chen Q, Masuda Y, Takegoshi K, Amoureux JP (2012) Very-long-distance correlations in proteins revealed by solid-state NMR spectroscopy. ChemPhysChem 13(16):3585–3588

Ishii Y (2001) C-13–C-13 dipolar recoupling under very fast magic angle spinning in solid-state nuclear magnetic resonance: applications to distance measurements, spectral assignments, and high-throughput secondary-structure determination. J Chem Phys 114:8473–8483

Ladizhansky V (2009) Homonuclear dipolar recoupling techniques for structure determination in uniformly C-13-labeled proteins. Solid State Nucl Magn Reson 36(3):119–128

Luo W, Hong M (2006) Determination of the oligomeric number and intermolecular distances of membrane protein assemblies by anisotropic ^1H-driven spin diffusion NMR spectroscopy. J Am Chem Soc 128(22):7242–7251

Marulanda D, Tasayco ML, McDermott A, Cataldi M, Arriaran V, Polenova T (2004) Magic angle spinning solid-state NMR spectroscopy for structural studies of protein interfaces. Resonance assignments of differentially enriched *Escherichia coli* thioredoxin reassembled by fragment complementation. J Am Chem Soc 126(50):16608–16620

McDermott A (2009) Structure and dynamics of membrane proteins by magic angle spinning solid-state NMR. Annu Rev Biophys 38:385–403

Morcombe CR, Gaponenko V, Byrd RA, Zilm KW (2004) Diluting abundant spins by isotope edited radio frequency field assisted diffusion. J Am Chem Soc 126(23):7196–7197

Renault M, Cukkemane A, Baldus M (2010) Solid-state NMR spectroscopy on complex biomolecules. Angew Chem Int Ed 49(45):8346–8357

Rienstra CM et al (2002) De novo determination of peptide structure with solid-state magic-angle spinning NMR spectroscopy. Proc Natl Acad Sci USA 99(16):10260–10265

Scholz I, Huber M, Manolikas T, Meier BH, Ernst M (2008) MIRROR recoupling and its application to spin diffusion under fast magic-angle spinning. Chem Phys Lett 460(1–3):278–283

Sun SJ, Butterworth AH, Paramasivam S, Yan S, Lightcap CM, Williams JC, Polenova T (2011) Resonance assignments and secondary structure analysis of dynein light chain 8 by magic-angle spinning NMR spectroscopy. Can J Chem 89(7):909–918

Sun SJ, Han Y, Paramasivam S, Yan S, Siglin AE, Williams JC, Byeon IJL, Ahn J, Gronenborn AM, Polenova T (2012a) Solid-state NMR spectroscopy of protein complexes. Protein NMR Techniques. Humana Press, New Jersey, pp 303–331

Sun SJ, Yan S, Guo CM, Li MY, Hoch JC, Williams JC, Polenova T (2012b) A time-saving strategy for MAS NMR spectroscopy by combining nonuniform sampling and paramagnetic relaxation assisted condensed data collection. J Phys Chem B 116(46): 13585–13596

Szeverenyi NM, Sullivan MJ, Maciel GE (1982) Observation of spin exchange by two-dimensional fourier transform C-13 cross polarization magic-angle spinning. J Magn Reson 47(3):462–475

Takegoshi K, Nakamura S, Terao T (2001) C-13–H-1 dipolar-assisted rotational resonance in magic-angle spinning NMR. Chem Phys Lett 344(5–6):631–637

Tycko R (2011) Solid-state NMR studies of amyloid fibril structure. Annu Rev Phys Chem 62:279–299

Veshtort M, Griffin RG (2011) Proton-driven spin diffusion in rotating solids via reversible and irreversible quantum dynamics. J Chem Phys 135:134509

Weingarth M, Bodenhausen G, Tekely P (2009) Broadband carbon-13 correlation spectra of microcrystalline proteins in very high magnetic Fields. J Am Chem Soc 131:13937–13939

Weingarth M, Bodenhausen G, Tekely P (2010) Broadband magnetization transfer using moderate radio-frequency fields for NMR with very high static fields and spinning speeds. Chem Phys Lett 488(1–3):10–16

Williams JC, Roulhac PL, Roy AG, Vallee RB, Fitzgerald MC, Hendrickson WA (2007) Structural and thermodynamic characterization of a cytoplasmic dynein light chain-intermediate chain complex. Proc Natl Acad Sci USA 104(24):10028–10033

Yang J, Tasayco ML, Polenova T (2008) Magic angle spinning NMR experiments for structural studies of differentially enriched protein interfaces and protein assemblies. J Am Chem Soc 130(17):5798–5807